Investigation of Photocatalytic and Seed Germination Effects of TiO$_2$ Nanoparticles Synthesized by *Melia azedarach* L. Leaf Extract

Muhammad Rafique[1] · **Javeria Jahangir**[1] · **Bilal Ahmad Zafar Amin**[2] · **M. Bilal Tahir**[1] · **Ghulam Nabi**[1] · **M. Isa Khan**[1] · **N. R. Khalid**[1] · **S. S. A. Gillani**[3] · **Iqra Sadaf**[1]

Abstract

The captivating properties and versatile applications of TiO$_2$ nanoparticles make them one of the emerging and widely used nanomaterials in current era. Green synthesis of nanoparticles is normally exploited to ensure environment friendly route and as potential candidate in their applications. In this work, owing to the sensitive applications of TiO$_2$ nanoparticles in water purification and agriculture, green synthesis was preferred using leaf extract of *Melia azedarach* L. as reducing and capping agent. Optical, structural and morphological properties of the synthesized nanoparticles were examined by UV–Vis spectroscopy, X-ray diffraction (XRD) and scanning electron microscopy (SEM) respectively, which revealed their crystallinity and spherical shape with 50–71 nm size. Functional groups responsible for the effective fabrication and stability of nanoparticles were indicated by Fourier transform infrared (FTIR) spectroscopy and purity of synthesized nanoparticles was analysed by Energy Dispersive X-ray (EDX) spectroscopy. Nanoparticles were found to be pure, well dispersed and rutile in nature. TiO$_2$ nanoparticles exhibited efficient degradation of Eosin dye, demonstrated as prototype of polluted water. Moreover, TiO$_2$ nanoparticles were also found quite efficient in enhancing germination of *Pennisetum glaucum* seeds and represented germination index of 89.3. Therefore, green synthesized TiO$_2$ nanoparticles by *Melia azedarach* L. extract can be employed as fertilizing and catalysing agents in the field of food and agriculture and as decontaminating and purifying agents in the field of environmental purification as future prospects.

Keywords Green synthesis · Nanoparticles · Photocatalytic activity · Seed germination · TiO$_2$ nanoparticles

1 Introduction

Environmental, especially, aquatic pollution is the major challenge for current era researchers due to rapid increase in population and industries. Therefore, wastewater treatments, particularly, catalytsis techniques, are gaining attention to control the aquatic pollution. A number of conventional physical, chemical and biological methods such as coagulation, adsorption and membrane separation were used for wastewater treatment, but, these methods convert organic contaminated water in solid form of membrane fouling and sludge [1–3]. The photocatalysis attracting attention of researchers for the treatment of organic, inorganic and heavy metals polluted wastewater without producing sludge and solid waste [4–8]. Photocatalysis depends upon the nature and properties of the photocatalysts like band gap, recombination rate, electron–hole pair production and stability. TiO$_2$ is the most widely reported photocatalyst due to its peculiar properties such as chemical stability, high oxidizing and photocatalytic activity [9]. Therefore, TiO$_2$ is utilized as standard photocatalyst in the degradation of organic dyes, environmental disinfection and hydrogen production [4, 5, 10]. Moreover, it is used in wide range of applications including water treatment, deodorization, air purification, cosmetics, self-cleaning agent in paints and coating, energy production and storage applications, pharmaceutical applications, food packing and storage [11, 12]. Instead of using different methods, the interest is shifting to green synthesis of photocatalysts to eliminate many hazardous effects during

✉ Muhammad Rafique
mrafique.uet@gmail.com

1 Department of Physics, University of Gujrat, Gujrat 50700, Pakistan

2 Department of Environmental Science, Abbottabad Campus, COMSATS University, Islamabad, Pakistan

3 Department of Physics, Government College University, Lahore, Pakistan

their utilization in different applications. Therefore, many research groups are working on green synthesis of TiO_2 nanostructures for photocatalytic activity by using different plants and their extracts such as *Nyctanthes arbor-Tristis* [13], *Jatropha curcas L. latex* [14], *Psidium guajava* [15], *Trigonella foenum-graecum* [16] *Deparia boryana* [17] and *Sesbania grandiflora* [18].

Furthermore, nanoparticles are used in the agriculture field to detect pathogens, improve plant production, to enhance growth rate and seed germination, and retention of herbicides and pesticides in crops [19]. It is investigated that, TiO_2 nanoparticles exhibited appreciable seed germination, root length, shoot length and vigorous index for various plants such as coriander plant [20], *Vigna radiate* L. (mung bean) [21], *Oryza sativa* L. (rice) seedlings, *Brassica napus* (canola) seeds [22, 23] and *Triticumaestivum* L. (wheat) plants) [24]. Therefore, TiO_2 nanoparticles can be trusted as a green aiding substance by agriculturalists.

In present study, TiO_2 nanoparticles are effectively synthesized by using leaf extract of *Melia azedarach* L. which have not yet been reported elsewhere. The reported plant is preferred due to its widespread diversity, medicinal nature and appropriate composition as it contains terpenoids, polyphenols, alcohols, lipids, alkaloids and tannins and helps to reduce bulk TiO_2 into nanoparticles. The prepared TiO_2 was effectively used for photocatalytic degradation of 5000 ppm Eosin dye textile polluted water. Moreover, the synthesized TiO_2 nanoparticles were used as appealing fertilizer in the filed agriculture and *Pennisetum glaucum* seeds were tested for the seed germination growth parameter at room temperature.

2 Materials and Methods

2.1 Synthesis of TiO_2 Nanoparticles

Fresh leafs of *Melia azedarach* L. were collected from rural area of Gujrat city, Pakistan. Leaf were surface cleaned with running tap water thrice followed by distilled water rinsing. Washed leaf were air dried in clean and ambient environment. 10 g of leaves, weighed by digital weighing balance were boiled in 100 ml of distilled water at 60 °C for 10 min to kill pathogens. The leaf extract was filtered through Whatsman filter paper No. 1 and was cooled down to room temperature. TiO_2 powder was purchased from Sigma Aldrich and 5 mM precursor solution was prepared. 10 ml of aqueous leaf extract was added in 90 ml of 5 mM TiO_2 solution and the mixture was homogenously stirred for 6 h at 60 °C. After stirring, the change in colour of solution (greenish brown colour) indicated the reduction of TiO_2 powder into TiO_2 nanoparticles. The extract ratio was varied (Table 1) to check the effect of extract concentration

Table 1 Details of leaf extract and precursor solution

Samples	Leaf extract (ml)	Precursor solution (ml)
1	5	90
2	10	90
3	15	90
4	20	90
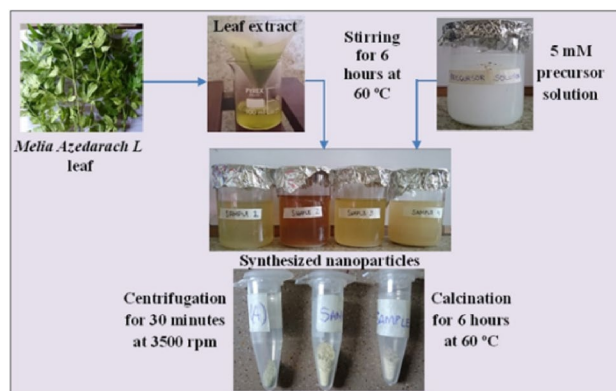
Fig. 1 Stepwise experimentation flowchart for green synthesis of TiO_2 nanoparticles

on properties of synthesized nanoparticles to ensure best combination for use in selected applications.

The stirred solution was centrifuged at 3500 rpm for 30 min. The centrifuged precipitates were washed by distilled water to remove impurities and were calcinated in thermostatic drying oven at 60 °C for 4 h to extract the required nanoparticles. Stepwise experimentation is given in Fig. 1.

2.2 Photocatalytic Dye Degradation

Photocatalytic applications of TiO_2 nanoparticles have been in use since long for environmental purification [25] by bacteria destruction [25], oxidation of contaminants like dye residues, organic films, etc. [26]. In present experimentation, TiO_2 nanoparticles are reported to degrade Eosin dye, present in Red fountain pen ink. 10 mg of TiO_2 nanoparticles (sample 3) having 57–64 nm size were used against 10 ml of artificially designed industrial waste water containing Eosin dye (1 ppm solution of Eosin dye). The solution was exposed to visible light but no significant degradation was observed under visible light range. However, in the presence of Ultraviolet (UV) light source, TiO_2 nanoparticles acted efficiently as photo catalyst and degraded the dye. This reveals their effectiveness in water treatment to ensure clean and pollutant free water.

2.3 Seed Germination

Fresh, undamaged millet seeds were purchased from commercial seed store, washed thrice with distilled water followed by filtration and air drying. Three sampling sets were prepared, first being the 'Control sample' treated with distilled water while second and third samples were treated with bulk TiO_2 powder solution and TiO_2 nanoparticles solution, respectively. 5 mg/L solutions of P25 (bulk TiO_2) and TiO_2 nanoparticles were prepared in distilled water for the treatment. The seeds were kept soaked for 24 h in their corresponding solutions. After 24 h, seeds were carefully transferred to moist filter paper containing petri dishes via tongs. The seeds were placed apart from each other in petri dishes to visualize the germination process clearly and were foliar sprayed by 10 ml of their mother solutions before sealing the petri dishes. The petri dishes were kept in Nanolaboratory's authorized lockers at 25 °C temperature and are shown in Fig. 2. The experimental observation tenure was kept 7 days. Various parameters like root length, shoot length, germination percentage, germination rate, and seed vigor index were recorded. The germination progress for control sample, bulk TiO_2 and TiO_2 nanoparticles was compared to analyze their corresponding effects and to check the difference of employing TiO_2 nanoparticles in this respect.

2.4 Characterization Techniques

The synthesized TiO_2 nanoparticles were characterized by UV–Vis spectrophotometer (UV-1700, Shimadzu), XRD (KAPPA APEX II (Cu-α, $\lambda = 1.54$ Å)) and SEM (TESCAN MIRA3) to study their optical, structural, and morphological properties, respectively. FTIR spectroscopy and EDX analysis were employed to check their surface and elemental purity.

3 Results and Discussion

3.1 UV–Vis Spectroscopy and Optical Properties

Optical properties like absorption and band gap of synthesized TiO_2 nanoparticles were investigated by UV–Vis absorption spectra. In UV–Vis spectroscopy, the absorption wavelength and intensity always depend upon a number of parameters like particle size, concentration, temperature etc. [27]. In solvents with high dielectric constant, the dissolution causes shift towards longer wavelengths and is termed as 'red shift' or bathochromic shift. This shift gives information about the size, material and hence band gap of the of synthesized nanoparticles, whereas the height of the absorption peak is directly proportional to concentration of sample [28]. UV–Vis absorption spectra of *Melia Azedarach* L. leaf extract in inset of Fig. 3 and TiO_2 nanoparticles are shown in Fig. 3. The absorption band edges of the samples are in range of 250–400 nm with slight variations in absorption magnitude and width of peak which are in well agreement with reported literature [29–31]. By analysing the absorption edge of peaks, we observed that with the increase in concentration of leaf extract, the corresponding absorption band edge wavelengths were increased. In all samples, the precursor ratio was kept constant while extract ratio was increased. The purpose of varying the extract ratio was to
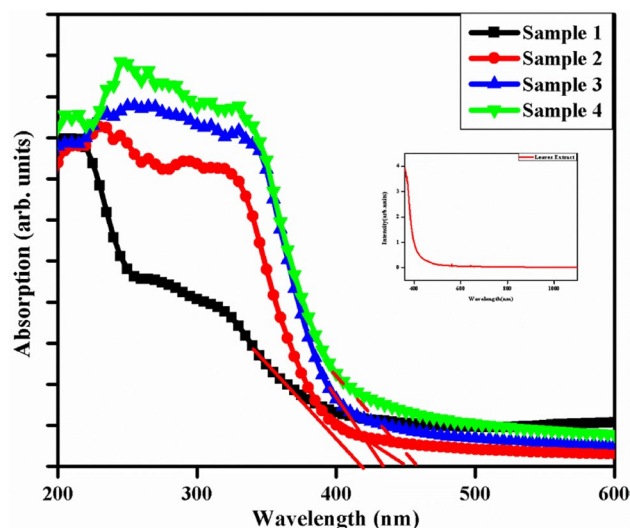

Fig. 2 Images of 7 days germinated Pennisetum glaucum seeds

Fig. 3 UV–Vis absorption spectra of TiO_2 nanoparticles synthesized using different concentrations of leaf extracts and absorption spectrum of leaf extract of *Melia Azedarach* L. (inset)

optimize the synthesis mechanism and to figure out the best combination for optimized synthesis of nanoparticles.

The band gap energy (E_g) of the TiO_2 nanoparticles was determined by both direct and indirect methods. In direct method, the tangent was plotted at the absorption band which gave the corresponding wavelength (Table 2). In indirect method, Tauc plots were taken and extrapolation of straight line gave E_g of corresponding bands as shown in Fig. 4 [32]. The Tauc relation can be expressed by Eq. 1 [33].

$$\alpha h\upsilon = A(h\upsilon - Eg)^{n/2} \tag{1}$$

Here α is absorption coefficient and can be calculated from Eq. 2 [33], h and υ are Plank constant and frequency respectively. A is band tailoring constant, Eg is the band gap energy and n represent the transition i.e. 1 for the direct transition.

$$\alpha = \frac{4\pi k}{\lambda} \tag{2}$$

Where k is extinction coefficient and λ is the wavelength of the incident light. Both direct and indirect transition band gaps were calculated by Tauc relation, but the indirect band gap energies were discarded due to mismatch with directly calculated band gap from UV–Vis absorption spectra. The calculated direct transition band gaps are shown in Table 2. It can be observed that with an increase in extract ratio the band gap also increased due to decrease in size of the nanoparticles.

3.2 Fourier Transform Infrared Spectroscopy (FTIR)

FTIR spectroscopy was employed for investigation of the functional groups present in the samples and their possible role towards the green action i.e. to see the various constituents present in plant extract which play the role of metal ion reduction and act as capping agent in the synthesis of TiO_2 nanoparticles. The FTIR spectra of the prepared samples are shown in Fig. 5.

The FTIR spectra of TiO_2 nanoparticle were recorded in range 500–4000 cm^{-1} and showed characteristic bands at 1091, 1225, 1332, 1376, 1531, 1587, 1657, 1766, 2361 and

Table 2 Band gap of TiO_2 nanoparticles calculated from the direct method (UV–Vis absorption spectra) and from Tauc relation

Sample	Band gap calculated from UV–Vis spectra (eV)	Band gap calculated from Tauc plots (eV)
1.	2.97	2.99
2.	2.76	2.60
3.	2.85	2.85
4.	2.70	2.70
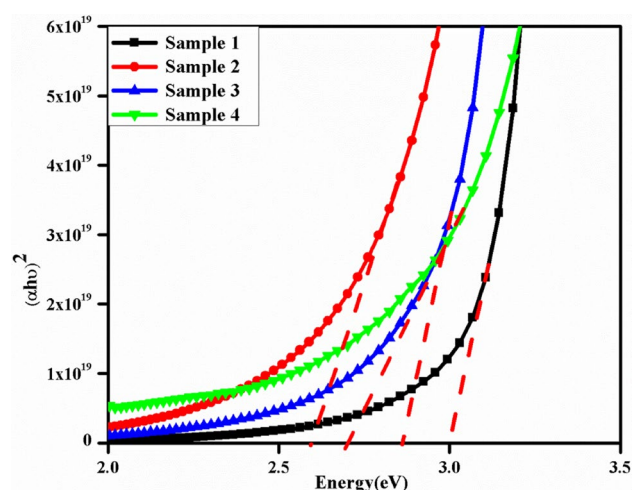
Fig. 4 Tauc plots along with tangents for TiO_2 nanoparticle*s*

3284 cm^{-1}. Band at 1091 cm^{-1} corresponded to C-O stretching vibrations that reveal the presence of saturated secondary alcohols present in leaf extract of *Melia azedarach* L. Similarly, the band at 1225 cm^{-1} indicated the presence of free amino acids. Phenol combination of O–H deformation vibration and C–O stretching vibration were found at 1332 cm^{-1} and 1376 cm^{-1}, respectively. 1531 cm^{-1} is referred to presence of C=N stretching and indicated metal with C=C stretching vibrations. 1587 cm^{-1} band directly reported the presence of heavy element or compound and the only heavy element present in the sample was Ti or TiO_2. The metallic indication, combined with the heavy element prediction revealed the presence of synthesized TiO_2 nanoparticles. Flavones were detected by C=O vibration at 1657 cm^{-1}
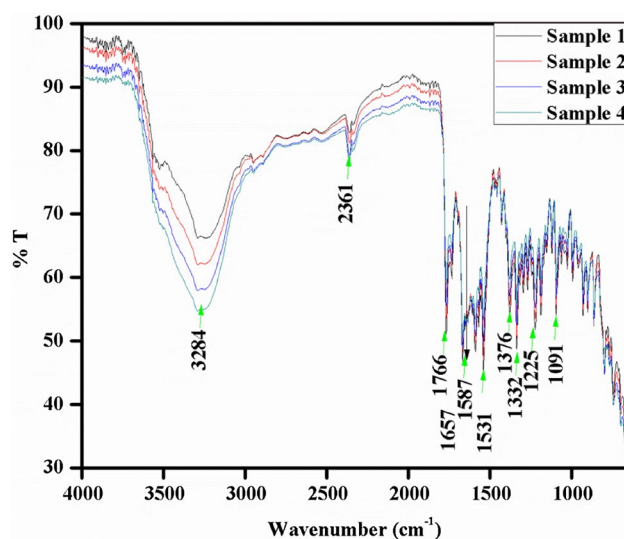
Fig. 5 FTIR spectra of TiO_2 nanoparticles synthesized by leaf extracts

which are reported to be active reducing agents, present in plant extract, that help in the synthesis of nanoparticles. Lactones and saturated aliphatic compounds (hydrocarbons) were identified at 1766 cm^{-1} and broad O–H vibrations in solid phase were significant at 2361 cm^{-1}. In the same way, hydrogen bonding was detected in various constituents like carboxylic acid; water etc. at 3284 cm^{-1}. In addition, polypeptides which indicate the presence of proteins were also detected in the form of N–H stretching vibration.

Thus, with the help of FTIR spectroscopy, it was evident that alcohols, phenols, aliphatic hydrocarbons and flavones were present in the sample, donated by leaf extract which act as reducing and capping agents in green synthesis of nanoparticles. These groups caused bio-reduction of TiO$_2$ nanoparticles as indicated by the same FTIR spectroscopy corresponding to wavenumbers 1531 cm^{-1} and 1587 cm^{-1} and referred to metallic presence as well as heavy element or group with heavy element.

The leaf extract of *Melia Azedarach* contains phytochemicals such as steroids, phenols, alkaloids, tannins, flavonoids, saponins and terpenoids, which are acting as oxidizing and reducing agent in green synthesis of TiO$_2$ NPs. The presence of these phytochemicals were investigated through phytochemical screening test as reported in literature [34–36].

3.3 X-ray Diffraction

The prepared samples were also examined by XRD to explore the structural and crystallographic properties of TiO$_2$ nanoparticle and the results are shown in Fig. 6. The graph shows diffraction peaks at 27.41°, 35.94°, 41.55°, 54.44° and 68.93° corresponding to (110), (101), (111),

(211) and (112) planes, respectively, which confirmed the rutile phase with tetragonal unit cell as per JCPDS card number 87-0920. This confirmation is also in agreement with reported literature [37, 38].
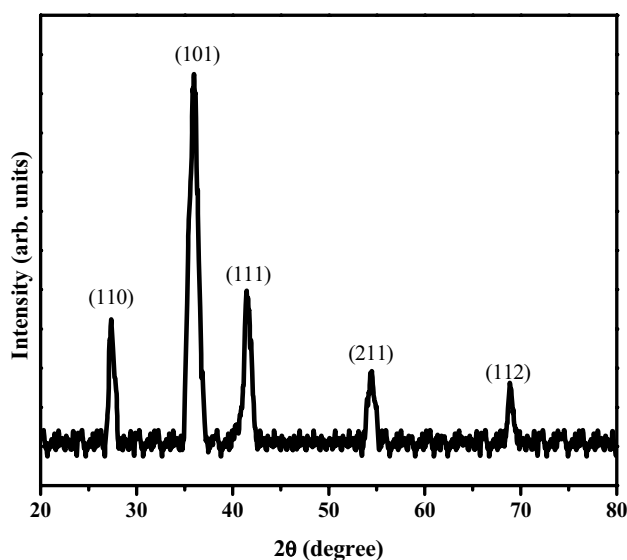
The crystallite size was calculated by using Scherer's formula in Eq. 3 [39].

$$\Gamma = \frac{K\lambda}{\beta \cos \theta} \tag{3}$$

where, Γ, K, λ, β, θ are mean size of crystalline domain, dimensionless shape factor (typically ≈ 0.9), X-ray wavelength, line broadening, Bragg's angle, respectively. The crystallite size using Scherer's formula was calculated corresponding to each plane and it varied in a range of 9.18 nm to 18.80 nm as shown in Table 3.

TiO$_2$ exists in three crystalline phases i.e. anatase, rutile and brookite. It can be described with reference to TiO$_6$ octahedral with Ti at center and O at vertices where in each forms their sharing positions differ, each TiO$_6$ octahedra shares two edges in rutile, three in brookite while four in anatase [40] which render Rutile and Anatase to be 'Tetragonal', while brookite to be 'Orthorhombic'. Despite the structural similarities between the three crystalline phases, their chemical and electronic properties differ significantly [41]. Among the three polymorphs of Titania, rutile is the most stable form, whereas the other two being unstable can transform to rutile depending on various parameters [42].

3.4 Scanning Electron Microscopy

Scanning electron microscopy was employed to study the size, shape of synthesized TiO$_2$ nanoparticles and to keenly analyse the effect of change in extract concentration on size, shape and appearance of synthesized nanoparticles. SEM micrographs of TiO$_2$ nanoparticles are shown in Fig. 7a–d.

Figure 7a shows the nanoparticles synthesized by 5 ml leaf extract. The nanoparticles had a wide size range and random shapes which were due to aggregation and agglomeration of the nanoparticles. Figure 7b shows nanoparticles synthesized by 10 ml leaf extract with size range of 64.94–78.45 nm and spherical like shape. All nanoparticles were monodispersed and had no agglomeration. Figure 7c shows the nanoparticles prepared by 15 ml leaf extract

Fig. 6 X-ray diffraction graph of TiO$_2$ nanoparticles

Table 3 XRD data and calculated parameters

Sr. No.	2θ	Plane	Crystallite size (nm)	Mean size (nm)
1	27.415	(110)	14.774661	13.45
2	35.946	(101)	9.1802922	
3	41.559	(111)	11.846089	
4	54.448	(211)	12.644807	
5	68.936	(112)	18.806056	

Fig. 7 SEM image of Synthesized TiO_2 nanoparticles with different leaf extract **a** 5 ml, **b** 10 ml, **c** 15 ml and **d** 20 ml
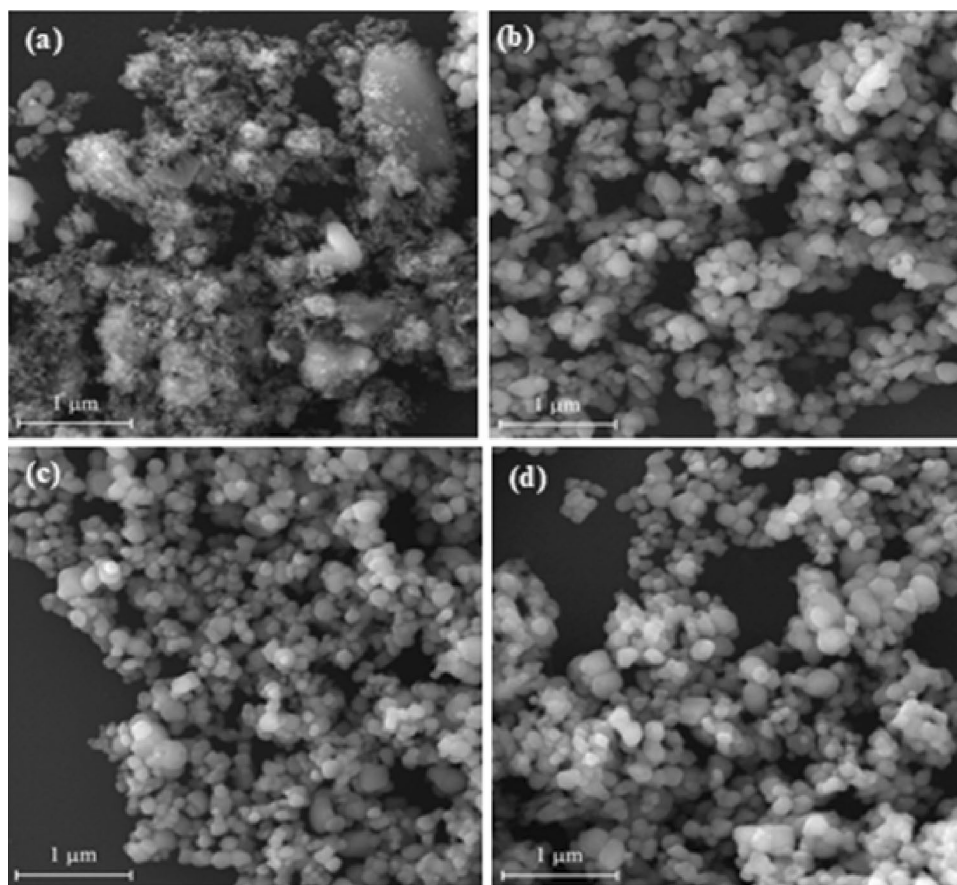
with spherical shape and size range of 57–64 nm and are nearly homogeneously dispersed. Figure 7d reports spherical and well dispersed nanoparticles with size range of 54.12–68.91 nm.

Overall SEM results revealed the decrease in size of nanoparticles with increase in plant extract ratio. This is due to the fact that with the increase in extract concentration, reducing and capping agents occurring naturally in plant extract also increase, that stabilize the synthesized nanoparticles more constructively. Hence, with the increase in extract ratio from 5 to 20 ml, corresponding size of synthesized nanoparticles got decreased from 71 to 50 nm and so did the agglomeration. Hence, leaf extract served as surfactant and stabilizer.

3.5 Energy Dispersive X-ray Spectroscopy (EDX)

The elemental analysis and verification of TiO_2 nanoparticles was performed by EDX and is shown in Fig. 8. The EDX spectra represented purity of synthesized TiO_2 nanoparticles, as only Titanium and Oxygen peaks were observed without impurity traces. The elemental weight and atomic percentage are given in Table 4. It also proves that after

washing there was no impurity, like extract or any other agent which could affect the applications.

3.6 Photocatalytic Test for Dye Degradation

In this study, photocatalytic properties of TiO_2 nanoparticles were evaluated for degradation of Eosin dye. The structure of Eosin dye is depicted in Fig. 9a. Eosin dye is from a class of dyes which are used in various industrial applications such as color filter, paper inks, textile, etc. The solution of Eosin dye was collected from textile industry in order to test photocatalytic activity of TiO_2 nanoparticles. An UV–Vis lamp with wavelength 365–450 nm was used in the catalytic activity.

Photocatalytic reactions are initiated due to electron hole pairs generation in the conduction and valence band of TiO_2 when irradiadted by UV light and the mechanism is shown in Fig. 9b. The conduction band electrons react with oxygen to produce superoxide anion radical and holes oxidize water molecules or hydroxide ion which is absorbed on the surface of TiO_2 nanoparticles. The steps involved in photocatalytic degradation of dye are given in Eqs. 4–12.
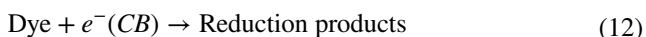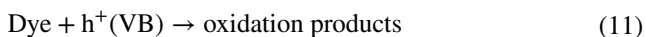
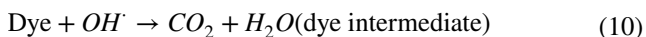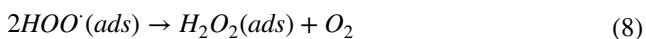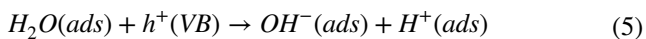$$TiO_2 + hv(UV) \rightarrow TiO_2\left(e^-(CB) + h^+(VB)\right) \tag{4}$$
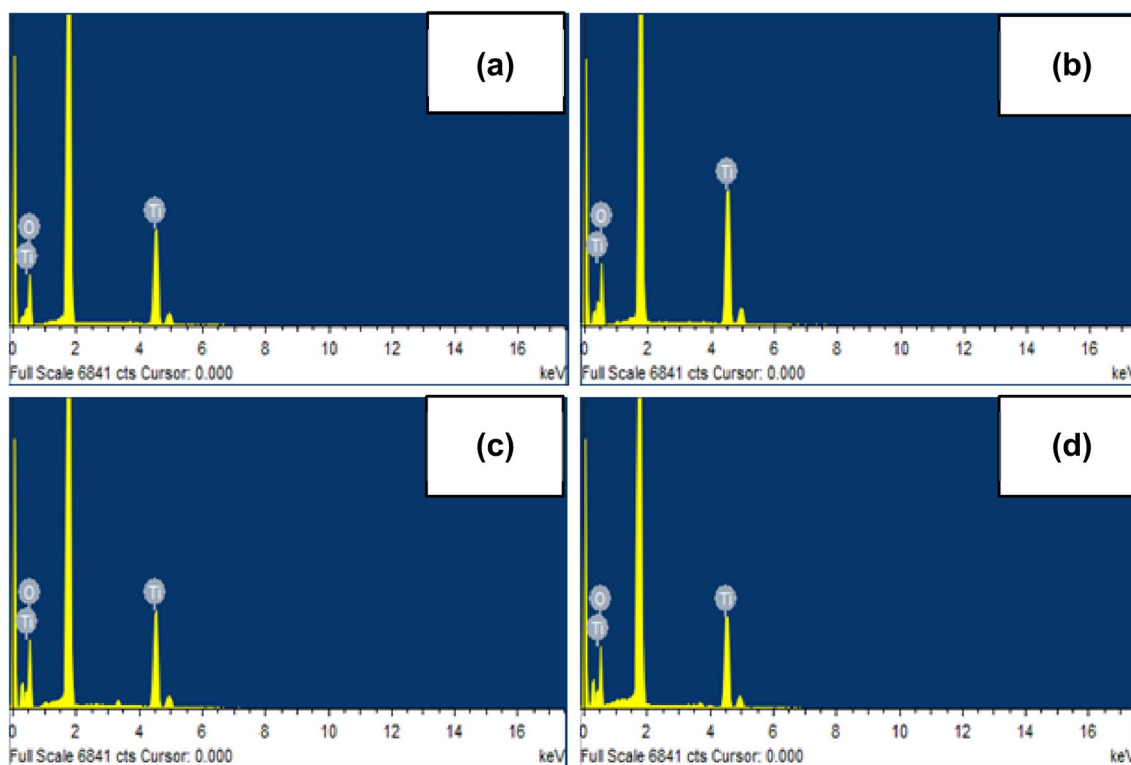
Fig. 8 EDX Spectrum of synthesized TiO$_2$ nanoparticles **a** 5 ml, **b** 10 ml, **c** 15 ml and **d** 20 ml leaf extract

Table 4 Elemental percentage from EDX

Sample	wt%		at.%	
	Ti K	O K	Ti K	O K
1	39.13	60.87	17.68	82.32
2	40.65	59.35	18.62	81.38
3	34.62	65.38	15.03	84.97
4	35.74	64.26	15.67	84.33

$$H_2O(ads) + h^+(VB) \rightarrow OH^-(ads) + H^+(ads) \tag{5}$$

$$O_2 + e^-(CB) \rightarrow O_2^{\cdot-}(ads) \tag{6}$$

$$O_2^{\cdot-}(ads) + H^+ \rightleftharpoons HOO^\cdot(ads) \tag{7}$$

$$2HOO^\cdot(ads) \rightarrow H_2O_2(ads) + O_2 \tag{8}$$

$$H_2O_2(ads) \rightarrow 2OH^\cdot(ads) \tag{9}$$

$$Dye + OH^\cdot \rightarrow CO_2 + H_2O(dye\ intermediate) \tag{10}$$

$$Dye + h^+(VB) \rightarrow oxidation\ products \tag{11}$$

$$Dye + e^-(CB) \rightarrow Reduction\ products \tag{12}$$

The photocatalytic action was represented by UV–Vis absorption spectra as shown in Fig. 10. It is clear in absorption spectra that by increasing UV exposure time the absorbance is decreased. The absorption of light depends on numbers of dye molecules that interact during exposure i.e. concentration of dye. If the dye solution is reasonably concentrated, it will have a high absorbance due to highest probability of interactions of dye molecules with incident light. Hence, it can be claimed that the decrease in absorption implies the decrease in concentration of dye in solution i.e. degradation of dye. It can be seen that with an increase in UV exposure time from 5 to 45 min, the absorption and hence the amount of dye present in artificially prepared industrial waste water decreased, which confirms that TiO$_2$ nanoparticles can be effectively used for photocatalytic dye degradation for water purification. The mechanism involves the excitation of electron from valence to conduction band of semiconductor on light exposure. Those excited electrons and positive holes in valence band cause oxidation of molecules around by transferring charge to surface of TiO$_2$.

3.6.1 Effect of pH

The photocatalytic activity of TiO$_2$ nanoparticles for an anionic dye is highly dependent on the pH of the solution. Figure 11 shows percentage removal efficiency of TiO$_2$ nanoparticles for Eosin dye at different pH (1–13), but, the removal efficiency for pH 1–7 are very low and are
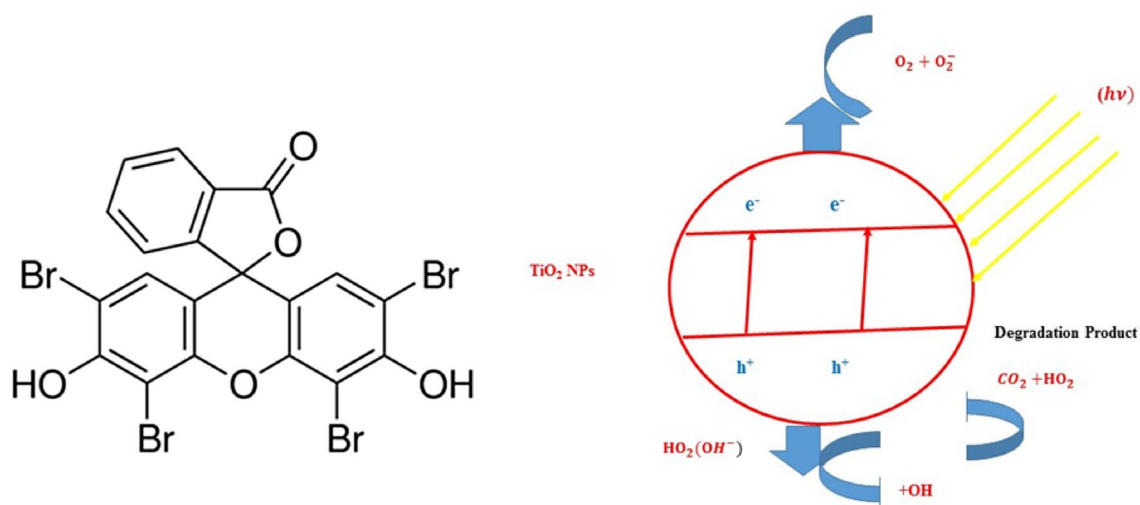
Fig. 9 **a** Structure of Eosin dye **b** Systemic representation of photocatalytic mechanism in degradation of Eosin dye with TiO_2 nanoparticles
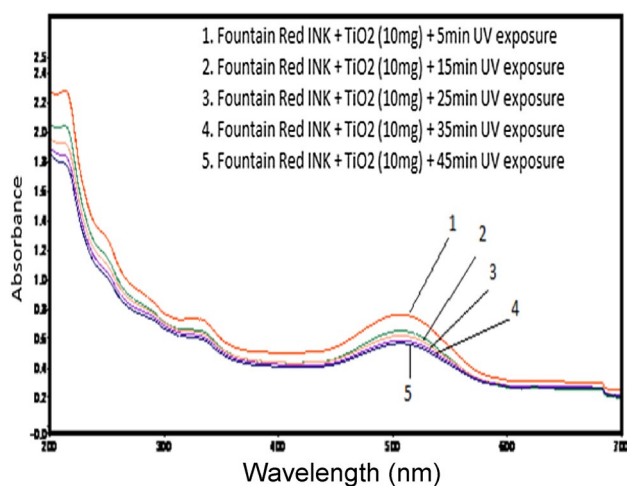

Fig. 10 UV–Vis absorption spectra of colloidal solution of Eosin dye and TiO_2 Nanoparticles under UV light exposure
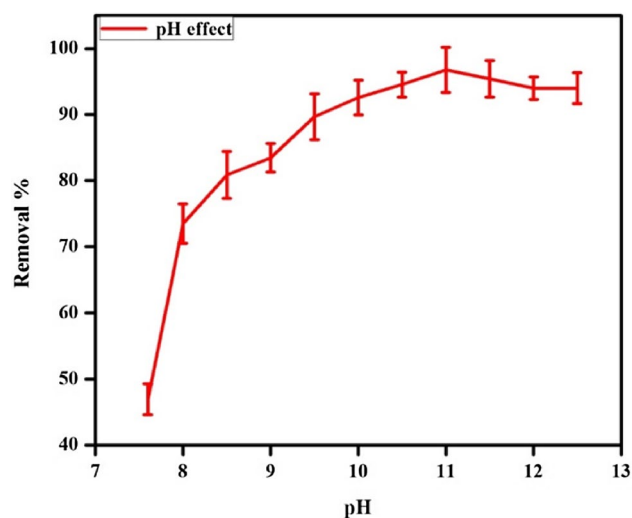
Fig. 11 pH effect on photocatalytic degradation of Eosin dye under UV light

not included in the graph. The removal efficiency has been observed to be 90% at pH 11 due to strong interaction of hydroxyl ions and the dye. The reaction time for each pH value was 20 min. The functional groups generated electrostatic charges on the surface of TiO_2 nanoparticles and dye through the process of deprotonation and protonation with respect to pH as given in Eqs. (13) and (14).

$$pH < pzc : TiOH + H^+ \rightarrow TiOH_2^+ \tag{13}$$

$$pH > pzc : TiOH + OH^- \rightarrow TiO^- + H_2O \tag{14}$$
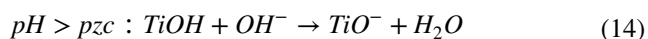
It is observed that photocatalytic degradation is sharply increased with increasing pH form 7–13 and maximum removal efficiency was obtained at pH 11 and further increase in pH tends to decrease photo degradation rate

as shown in Fig. 11 due to weaker electrostatic interaction between TiO_2 and dye.

3.6.2 Effect of Temperature

Temperature has been considered a vital aspect on studying photocatalytic activity of anionic dyes. The photocatalytic activity of Eosin dye as function of temperature was studied in the presence of TiO_2 catalyst under UV light irradiation and the reaction time for each measurement was 20 min. The increasing temperature tends to promote reaction efficiently with high electron hole pair recombination rate and results an increase in dye removal reaction rate. The photocatalytic activity of TiO_2 nanoparticles for Eosin dye on different

temperatures is shown in Fig. 12. It is evident that concentration of Eosin dye was gradually decreased on increasing temperature with maximum removal efficiency of 92% at 75 °C.

3.6.3 Effect of Catalyst Loading

The removal of dye was increased and controlled by the catalysts. However, some dyes can be degraded under light irradiation without any catalyst. Therefore, the removal of Eosin dye without catalyst, with TiO_2 catalyst and bulk TiO_2 (P25) is investigated and is shown in Fig. 13. It is also important to determine optimum amount of catalyst required to degrade maximum extent of dye under UV light at particular experimental conditions. It is clear that increasing amount of catalyst increased the removal efficiency of dye from 25 to 86%. The increase in removal efficiency is due to increasing number of active sites on the surface of photocatalyst TiO_2, which tends to increase number of superoxide and hydroxyl radicals. However, photocatalytic performance of bulk TiO_2 powder (P25) is observed only 46% which is limited due to its photo-responsive range and the results are also consistent with literature [43, 44].

3.6.4 Kinetic Study

The photocatalytic degradation process of Eosin textile pollutant dye was a pseudo first order by a linear correlation of $(\ln (C/C_0))$ with corresponding reaction time as depicted in Fig. 14. The calculated pseudo first order rate constant (k) is 0.0054 min^{-1} by using following equation.

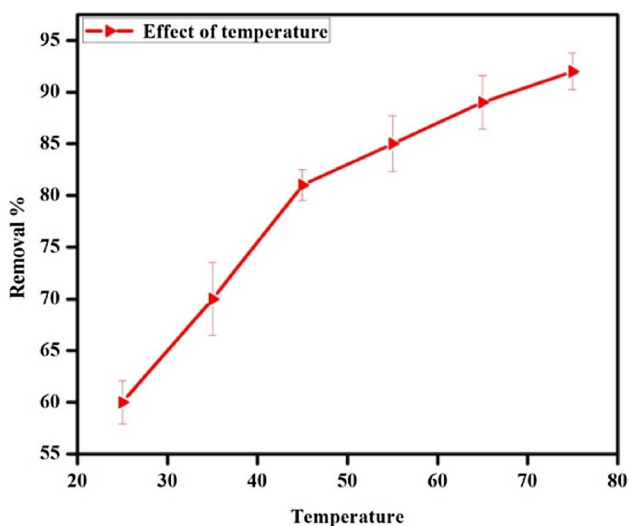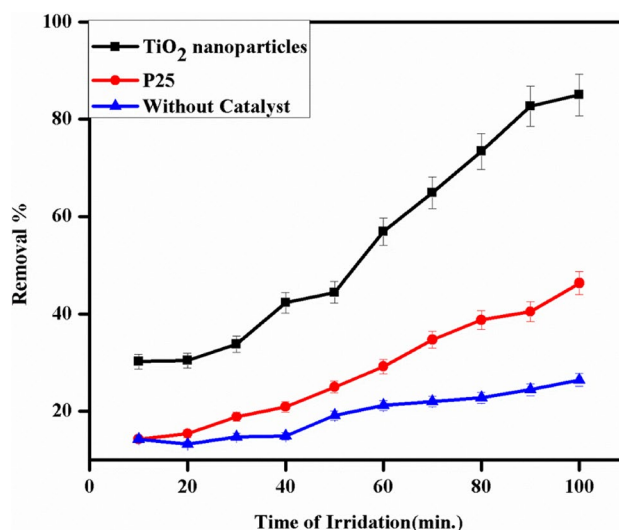$$\ln \left(\frac{C}{C_\circ} \right) = -kt \qquad (15)$$

Fig. 13 Effect of loading catalyst and P25 on photocatalytic degradation of Eosin dye under UV light

TiO2 Nanoparticles as nano-catalyst exhibited very good cyclic evaluation with 98% removal efficiency after five cycles. The recycle evaluation of optimal TiO_2 Nanoparticles with corresponding number of cycles is shown in Fig. 15.

3.7 Seed Germination Effects of TiO_2 Nanoparticles

The root and shoot lengths were measured by using sliding callipers. The root length is the distance of the root tip from root base, whereas shoot length is the distance of shoot tip from shoot base [22]. The germination percentage (GP) [22],
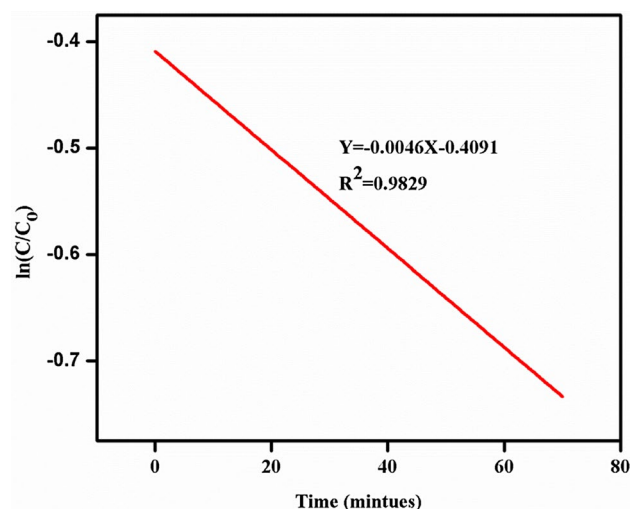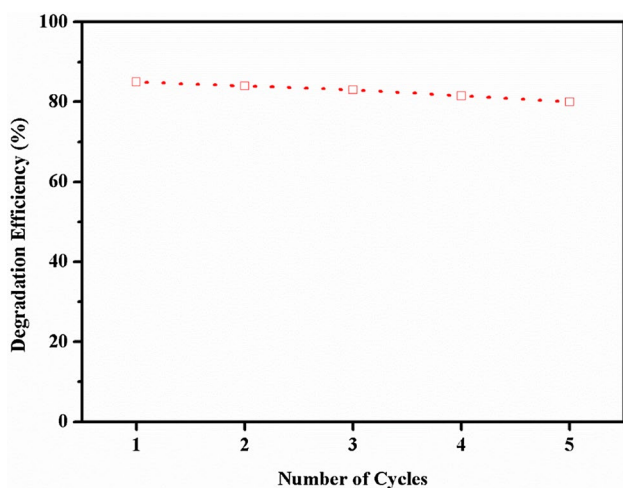

Fig. 12 Effect of temperature on photocatalytic degradation of Eosin dye under UV light

Fig. 14 Photodegradation process was to be pseudo first order as presented by correlation of $(\ln (C/C_0))$ with corresponding reaction time

Fig. 15 Recycle performance of optimal TiO$_2$ nanocatalyts with corresponding number of cycles

germination rate (GR) [23, 45], mean germination time (MGT) and seed vigor index (SVI) [46] were calculated by Eqs. 16, 17, 18 and 7, respectively and are presented in Fig. 16 and Table 5.
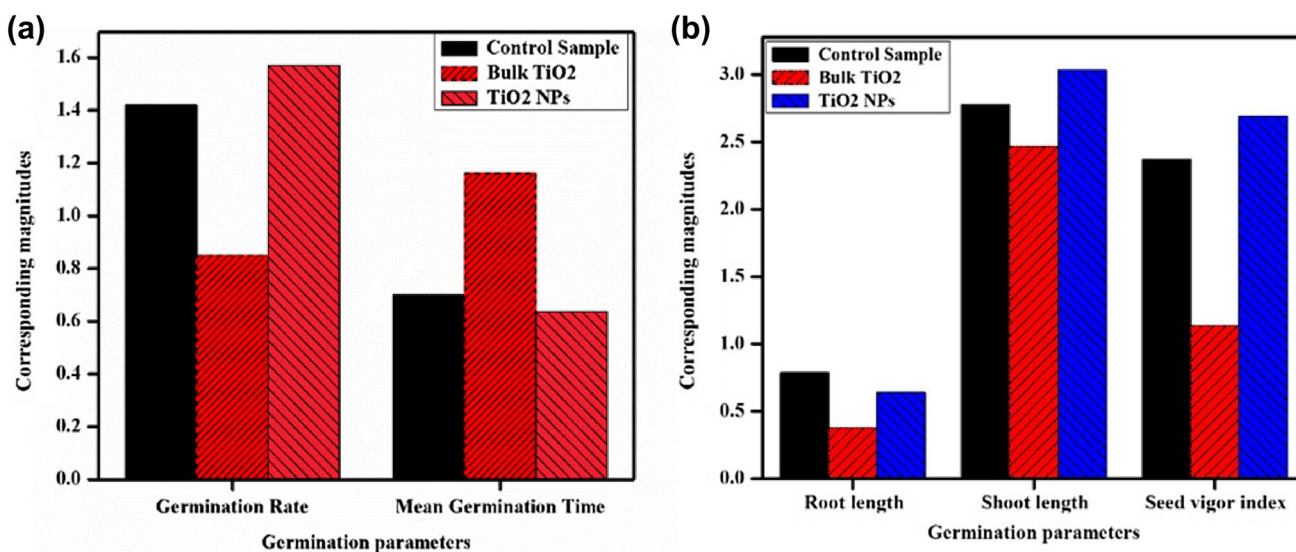
$$GP = \frac{\text{Number of germinated seeds}}{\text{Number of inoculated seeds}} \times 100 \qquad (16)$$

$$GR = \frac{\sum Gi}{I} \qquad (17)$$

where Gi represents the number of germinations on day i (i = 1,2,.....,7), $\sum Gi$ gives total germinations in 7 days and 'I' is total days i.e. 7.

$$MGT = \frac{\sum Gi}{\sum G} \times I \qquad (18)$$

$$SVI = GP \times (\text{shoot length} + \text{root length}) \qquad (19)$$

Fig. 16 **a** Length parameters of germinated seeds **b** Germination parameters of germinated seeds

Table 5 Germination parameters calculated for *Pennisetum glaucum* seeds

Sample type	Root length (inch)	Shoot length (inch)	Germination percentage	Germination rate	Mean germination time (days)
Control sample	0.785	2.777	66.66	1.42	0.7
Bulk TiO$_2$	0.380	2.464	40	0.85	1.16
TiO$_2$ NPs	0.638	3.033	73.33	1.57	0.636

Sample type	Seed vigor index	Relative root elongation	Relative seed germination	Germination index
Control sample	2.372	Reference	Reference	Reference
Bulk TiO$_2$	1.137	48.40	60	29.04
TiO$_2$ NPs	2.690	81.27	110	89.3

The net germination effect due to treatment can be calculated from the relative germination parameters with reference to control sample. Therefore, the relative root elongation (RLE), relative seed germination (RSG) and germination index (GI) were calculated from Eqs. 20, 21 and 22, respectively [47]. A comparison among the calculated parameters is shown in Fig. 14.

$$RLE = \frac{Mean\ root\ length\ with\ nanoparticles/bulk}{Mean\ root\ length\ with\ control} \times 100 \tag{20}$$

$$RSG = \frac{Seeds\ germinated\ with\ nanoparticles/bulk}{Seeds\ germinated\ with\ control} \times 100 \tag{21}$$

$$GI = \frac{RLE \times RSD}{100} \tag{22}$$

It is observed that all parameter like shoot length, germination percentage, germination rate, mean germination time and seed vigor index were influenced appreciably when treated with TiO_2 nanoparticles as compared to bulk TiO_2 and control sample. For all parameter, it was revealed that bulk TiO_2 powder had adverse effects on the germination while TiO_2 nanoparticles had increased the germination of the seeds.

4 Conclusion

TiO_2 nanoparticles have been synthesized by facile, cost effective and eco-friendly green route by using leaf extract of *Melia azedarach* L. The optical, structural, morphological and elemental properties of the synthesized TiO_2 nanoparticles were analysed by UV–Vis spectroscopy, XRD, SEM, EDX and FTIR, respectively. TiO_2 nanoparticles showed SPR peaks in the range of 209–249 nm with corresponding band gap of 3.03–3.20 eV. XRD results revealed TiO_2 nanoparticles to be rutile with tetragonal geometry. FTIR showed that alcohols, phenols, proteins and flavones were present in the extract of the leaf which reduced and stabilized the TiO_2 nanoparticles. The SEM results, coupled with EDX, revealed that nanoparticles were pure, spherical in shape with size range of 50–71 nm. Furthermore, synthesized TiO_2 nanoparticles showed excellent photocatalytic activity against Eosin dyes and germination ability for *Pennisetum glaucum* seeds.

Compliance with Ethical Standards

References

1. G. Crini, E. Lichtfouse, Advantages and disadvantages of techniques used for wastewater treatment. Environ. Chem. Lett. **17**, 145–155 (2019)
2. T. Okuda, E.N. Ali, *Water and Wastewater Treatment Technologies* (Springer, New York, 2019), pp. 63–79
3. U. Baig, A. Matin, M. Gondal, S. Zubair, Facile fabrication of superhydrophobic, superoleophilic photocatalytic membrane for efficient oil-water separation and removal of hazardous organic pollutants. J. Cleaner Prod. **208**, 904–915 (2019)
4. M.-C. Wu, W.-K. Huang, T.-H. Lin, Y.-J. Lu, Photocatalytic hydrogen production and photodegradation of organic dyes of hydrogenated TiO2 nanofibers decorated metal nanoparticles. Appl. Surf. Sci. **469**, 34–43 (2019)
5. X. Zhu, K. Pathakoti, H.-M. Hwang, *Green synthesis, characterization and applications of nanoparticles.* (Elsevier, Amsterdam, 2019), pp. 223–263
6. X. Zhang, Y. Yang, W. Huang, Y. Yang, Y. Wang, C. He, N. Liu, M. Wu, L. Tang, g-C3N4/UiO-66 nanohybrids with enhanced photocatalytic activities for the oxidation of dye under visible light irradiation. Mater. Res. Bull. **99**, 349–358 (2018)
7. N. Liu, W. Huang, M. Tang, C. Yin, B. Gao, Z. Li, L. Tang, J. Lei, L. Cui, X. Zhang, In-situ fabrication of needle-shaped MIL-53 (Fe) with 1T-MoS2 and study on its enhanced photocatalytic mechanism of ibuprofen. Chem. Eng. J. **359**, 254–264 (2019)
8. X. Zhang, Y. Wang, F. Hou, H. Li, Y. Yang, X. Zhang, Y. Yang, Y. Wang, Effects of Ag loading on structural and photocatalytic properties of flower-like ZnO microspheres. Appl. Surf. Sci. **391**, 476–483 (2017)
9. *Applications of titanium dioxdie nanocoating*. Proceedings of the Nano-technology in environments conference, (2006)
10. O.K. Nayna, S.M. Tareq, *Nanotechnology in water and wastewater treatment* (Elsevier, Amsterdam, 2019), pp. 267–290
11. G. Wang, H. Wang, Y. Ling, Y. Tang, X. Yang, R.C. Fitzmorris, C. Wang, J.Z. Zhang, Y. Li, Hydrogen-treated TiO2 nanowire arrays for photoelectrochemical water splitting. Nano Lett. **11**, 3026–3033 (2011)
12. F. Petronella, A. Truppi, M. Striccoli, M.L. Curri, R. Comparelli, *Noble metal-metal oxide hybrid nanoparticles* (Elsevier, Amsterdam, 2019), pp. 373–394
13. M. Sundrarajan, S. Gowri, Green synthesis of titanium dioxide nanoparticles by Nyctanthes arbor-tristis leaves extract. Chalcogenide Lett. **8**, 447–451 (2011)
14. M. Hudlikar, S. Joglekar, M. Dhaygude, K. Kodam, Green synthesis of TiO₂ nanoparticles by using aqueous extract of *Jatropha curcas* L. latex. Mater. Lett. **75**, 196–199 (2012)
15. T. Santhoshkumar, A.A. Rahuman, C. Jayaseelan, G. Rajakumar, S. Marimuthu, A.V. Kirthi, K. Velayutham, J. Thomas, J. Venkatesan, S.-K. Kim, Green synthesis of titanium dioxide nanoparticles using Psidium guajava extract and its antibacterial and antioxidant properties. Asian Pacif J. Trop. Med. **7**, 968–976 (2014)
16. S. Subhapriya, P. Gomathipriya, Green synthesis of titanium dioxide (TiO₂) nanoparticles by Trigonella foenum-graecum extract and its antimicrobial properties. Microb. Pathog. **116**, 215–220 (2018)

17. A. Arora. Green synthesis of bimetallic nanoparticles using aqueous extract of Deparia boryana, a Himalyan pteridophyte to develop novel antimicrobial agent (2018)

18. M. Srinivasan, M. Venkatesan, V. Arumugam, G. Natesan, N. Saravanan, S. Murugesan, S. Ramachandran, R. Ayyasamy, A. Pugazhendhi, Green synthesis and characterization of titanium dioxide nanoparticles (TiO$_2$ NPs) using *Sesbania grandiflora* and evaluation of toxicity in zebrafish embryos. Process Biochem. **1**, 1 (2019). https://doi.org/10.1016/j.procbio.2019.02.010

19. L.R. Khot, S. Sankaran, J.M. Maja, R. Ehsani, E.W. Schuster, Applications of nanomaterials in agricultural production and crop protection: a review. Crop Prot. **35**, 64–70 (2012)

20. M. Khater, Effect of titanium nanoparticles (TiO$_2$) on growth, yield and chemical constituents of coriander plants. Arab. J. Nucl. Sci. Appl. **48**, 187–194 (2015)

21. R. Raliya, P. Biswas, J. Tarafdar, TiO$_2$ nanoparticle biosynthesis and its physiological effect on mung bean (Vigna radiata L). Biotechnol. Rep. **5**, 22–26 (2015)

22. Y. Hao, Z. Zhang, Y. Rui, J. Ren, T. Hou, S. Wu, M. Rui, F. Jiang, and L. Liu, Effect of Different Nanoparticles on Seed Germination and Seedling Growth in Rice. In *2nd Annual International Conference on Advanced Material Engineering (AME 2016)*, Atlantis Press

23. H. Mahmoodzadeh, M. Nabavi, H. Kashefi, Effect of nanoscale titanium dioxide particles on the germination and growth of canola (Brassica napus). J. Ornam. Hortic. Plants. **3**, 25–32 (2013)

24. H. Mahmoodzadeh, R. Aghili, Effect on germination and early growth characteristics in wheat plants (Triticumaestivum L) seeds exposed to TiO$_2$ nanoparticles. J. Chem. Health Risks (2018). https://doi.org/10.22034/jchr.2018.544054

25. P. Dhandapani, S. Maruthamuthu, G. Rajagopal, Bio-mediated synthesis of TiO2 nanoparticles and its photocatalytic effect on aquatic biofilm. J. Photochem. Photobiol., B **110**, 43–49 (2012)

26. C. Chen, C. Lu, Y. Chung, J. Jan, UV light induced photodegradation of malachite green on TiO2 nanoparticles. J. Hazard. Mater. **141**, 520–528 (2007)

27. T.A. Egerton, UV-absorption—the primary process in photocatalysis and some practical consequences. Molecules **19**, 18192–18214 (2014)

28. A. Primer, *Fundamentals of UV-Visible spectroscopy* (Hewlett-Packard publication, Copyright Hewlett-Packard Company, 1996)

29. R. Dobrucka, Synthesis of titanium dioxide nanoparticles using *Echinacea purpurea* herba (Spring 2017). Iran. J. Pharm. Res. **16**(2), 756–762 (2017)

30. R. Sankar, K. Rizwana, K.S. Shivashangari, V. Ravikumar, Ultra-rapid photocatalytic activity of *Azadirachta indica* engineered colloidal titanium dioxide nanoparticles. Appl. Nanosci. **5**, 731–736 (2014)

31. S. Ambika, M. Sundrarajan, [EMIM] BF 4 ionic liquid-mediated synthesis of TiO 2 nanoparticles using Vitex negundo Linn extract and its antibacterial activity. J. Mol. Liq. **221**, 986–992 (2016)

32. J. Tauc, Optical properties and electronic structure of amorphous Ge and Si. Mater. Res. Bull. **3**, 37–46 (1968)

33. M. Rafique, M.S. Rafique, S.H. Butt, U. Kalsoom, A. Afzal, S. Anjum, A. Usman, Dependence of the structural optical and thermo-physical properties of gold nano-particles synthesized by laser ablation method on the nature of laser. Optik-Int. J. Light Electron Opt. **134**, 140–148 (2017)

34. M.F. Ahmed, A.S. Rao, S.R. Ahemad, M. Ibrahim, Phytochemical studies and antioxidant activity of Melia azedarach Linn leaves by DPPH scavenging assay. Int. J. Pharm. Appl. **3**, 271–276 (2012)

35. D. Sharma, Y. Paul, Preliminary and pharmacological profile of Melia azedarach L.: an overview. J. Appl. Pharm. Sci. **3**, 133–138 (2013)

36. G. Nahak, R.K. Sahu, In vitro antioxidative acitivity of *Azadirachta indica* and Melia azedarach leaves by DPPH scavenging assay. Nat Sci. **8**, 22–28 (2010)

37. G. Rajakumar, A.A. Rahuman, B. Priyamvada, V.G. Khanna, D.K. Kumar, P.J. Sujin, *Eclipta prostrata* leaf aqueous extract mediated synthesis of titanium dioxide nanoparticles. Mater. Lett. **68**, 115–117 (2012)

38. K.G. Rao, C. Ashok, K.V. Rao, C.S. Chakra, V. Rajendar, Synthesis of TiO$_2$ nanoparticles from orange fruit waste. Int. J. Adv. Res. Phys. Sci. **2**, 1 (2015)

39. A. Patterson, The scherrer formula for X-ray particle size determination. Phys. Rev. **56**, 978 (1939)

40. M. Matsui, M. Akaogi, Molecular dynamics simulation of the structural and physical properties of the four polymorphs of TiO$_2$. Mol. Simul. **6**, 239–244 (1991)

41. X.-Q. Gong, A. Selloni, First-principles study of the structures and energetics of stoichiometric brookite TiO$_2$ surfaces. Phys. Rev. B **76**, 235307 (2007)

42. Q. Zhang, L. Gao, Preparation of oxide nanocrystals with tunable morphologies by the moderate hydrothermal method: insights from rutile TiO$_2$. Langmuir **19**, 967–971 (2003)

43. C. Tian, Q. Zhang, A. Wu, M. Jiang, Z. Liang, B. Jiang, H. Fu, Cost-effective large-scale synthesis of ZnO photocatalyst with excellent performance for dye photodegradation. Chem. Commun. **48**, 2858–2860 (2012)

44. H. Zhang, X. Lv, Y. Li, Y. Wang, J. Li, P25-graphene composite as a high performance photocatalyst. ACS Nano **4**, 380–386 (2009)

45. R.D.A. Jalill, R.S. Nuaman, A.N. Abd, Biological synthesis of Titanium Dioxide nanoparticles by *Curcuma longa* plant extract and study its biological properties. World Sci. News **49**, 204–222 (2016)

46. A.A. Abdul-Baki, J.D. Anderson, Vigor determination in soybean seed by multiple criteria 1. Crop Sci. **13**, 630–633 (1973)

47. Y.K. Mushtaq, Effect of nanoscale Fe$_3$O$_4$, TiO$_2$ and carbon particles on cucumber seed germination. J. Environ. Sci. Health A **46**, 1732–1735 (2011)